Nanoscale

ARTICLE

Optical Control of Mitochondrial Reductive Reactions in Living Cells using an Electron Donor-Acceptor Linked Molecule†

Received 00th January 20xx,
Accepted 00th January 20xx

DOI: 10.1039/x0xx00000x

www.rsc.org/

Yuta Takano,*[a,b] Reina Munechika,[c] Vasudevan Pillai Biju,[b] Hideyoshi Harashima,[c] Hiroshi Imahori,*[b,d] and Yuma Yamada*[c]

It has been known for decades that intracellular redox reactions control various vital functions in living systems, which include synthesis of biomolecules, modulation of protein functions, and cell signaling. Although there have been several reports on control of such functions using DNA and RNA, non-invasive optical control of biological functions is an important ongoing challenge. In this study, a hybrid of an electron donor-acceptor linked molecule based on a ferrocene(Fc)-porphyrin(ZnP)-fullerene(C_{60}) analogue and an elaborately designed nano-carrier, referred to herein as a MITO-Porter, resulted in a successful photoinduced intermolecular electron transfer reaction *via* the long-lived intramolecular charge separation, leading to site-specific reductive reactions in mitochondria of living HeLa cells. A Fc-ZnP-C_{60} linked molecule, **1-Oct**, was designed and prepared for taking advantage of the unique photophysical properties with excellent efficiency (i.e. a long lifetime and a high quantum yield) for photoinduced charge separation. The targeted delivery of **1-Oct** to mitochondria was accomplished by using a combination of the Fc-ZnP-C_{60} molecule and a drug delivery nano-carrier, MITO-Porter, that was recently established by our group for intracellular cargo delivery. The successful delivery of **1-Oct** by the MITO-Porter permitted the optically-controlled generation of O_2^- in mitochondria of HeLa cells and the following induction of apoptosis as a cell signalling response was observed in confocal laser microscopy experiments. The obtained results indicate that the use of an electron donor-acceptor system such as this can be a promising tool for the non-invasive triggering of redox-coupled cellular activities in living systems.

Introduction

Controlling of cellular functions by means of light is a fascinating methodology for cell engineering because it can achieve excellent spatiotemporal resolution on a nanometer scale and sub-millisecond time scale.[1,2] In this regard, considerable effort has been devoted to developing novel methods for the photocontrol of cellular activities, such as cell signaling, cell viability, and intracellular redox reactions.

Redox reactions are of importance in biological system for governing cellular functions.[3,4] Redox homeostasis in the cell is maintained by the total balance of oxidized and reduced species, such as molecular oxygen, thioredoxin, glutathione, and their derivatives.[5-7] Thus, manipulating redox reactions in a cell represents a promising approach for studies of biological mechanisms and for developing effective molecular tools for controlling cellular activities. General approaches to control redox balance and redox reactions in the cell are, in most cases, administering a dose of redox reagents to a cell or genetic modification aimed at controlling the activity of redox related enzymes.[4-8] Although these are promising approaches and some have already been approved for clinical applications, potential weak points include the fact that they lack site-specificity in the cell and a longer time lag between the treatment and response compared to light control methods.

Utilizing a photoinduced electron transfer (ET) reaction from an artificial molecule can be an effective way modulating cellular redox reactions *via* photocontrol.[8,9] It is known that superoxide (O_2^-) is generated as a result of biological ET reactions, and O_2^- from mitochondria triggers a variety of activities in a cell, including apoptotic cell death,[10,11] cell transformations,[12] or the regulation of cardiac rhythm.[13] Although KillerRed and certain porphyrin derivatives have been proposed as effective photosensitizers for generating O_2^- in the cell,[14,15] the generation of singlet oxygen ($^1O_2$), which can be formed *via* intermolecular energy transfer from a photoexcited sensitizer to $^3O_2$ would potentially accompany the illumination of the sensitizers.[16] Because $^1O_2$ can exert severe cytotoxic effects, even when generated in trace amounts,[16] development of $^1O_2$-free methods is highly desirable for the precise photocontrol of cellular redox

[a] Research Institute for Electronic Science, Hokkaido University, Kita-20 Nishi-10, Kita-ku, Sapporo 001-0020, Japan. tak@es.hokudai.ac.jp
[b] Institute for Integrated Cell-Material Sciences (WPI-iCeMS), Kyoto University, Sakyo-ku, Kyoto 606-8501, Japan. imahori@scl.kyoto-u.ac.jp
[c] Laboratory for Molecular Design of Pharmaceutics, Faculty of Pharmaceutical Sciences, Hokkaido University, Kita-12 Nishi-6, Kita-ku, Sapporo 060-0812, Japan. u-ma@pharm.hokudai.ac.jp
[d] Department of Molecular Engineering, Graduate School of Engineering, Kyoto University, Nishikyo-ku, Kyoto 615-8510, Japan.
†Electronic Supplementary Information (ESI) available: Detailed synthetic procedures, spectroscopic data, supplementary characterizations and analyses. See DOI: 10.1039/x0xx00000x

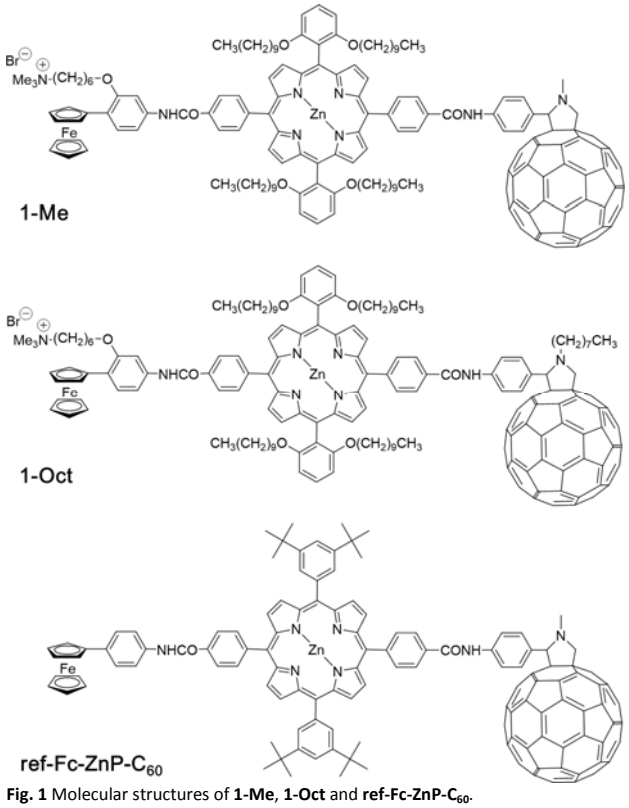

Fig. 1 Molecular structures of **1-Me**, **1-Oct** and **ref-Fc-ZnP-C_{60}**.

reactions and for accurately evaluating the effect of photocontrol. In addition, developing a versatile method for the intracellular site-specific delivery of a sensitizer would be highly desirable in terms of utilizing the full potential of photofunctional artificial molecules without undesired side-effects in cellular environments both *in vitro* and *in vivo*.

Our group recently reported on a new approach for the photocontrol of cellular activity. This strategy involves the use of a molecular system based on a ferrocene (Fc)-porphyrin (ZnP)-fullerene (C_{60}) analogue (**1-Me**)[17] (Fig. 1) whose molecular framework (**ref-Fc-ZnP-C_{60}**) was originally reported by us to show a highly efficient photoinduced intramolecular charge separation (CS) (Fc^{+}-ZnP-$C_{60}^{\bullet-}$) with a long lifetime and a high quantum yield ($\tau \sim 7.6$ μs, $\Phi = 0.99$ in benzonitrile).[18] Fc-ZnP-C_{60} analogue allowed us to take advantage of the unique photophysical phenomena associated with this molecule and to develop an intermolecular ET reaction involving the efficient

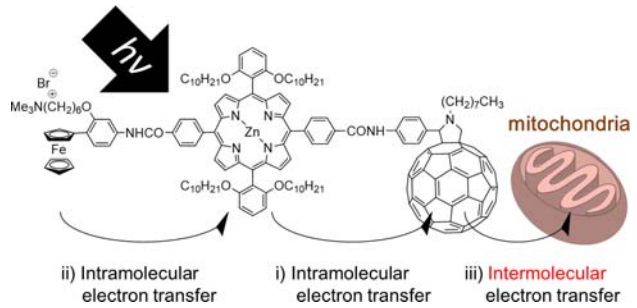

Fig. 2 Schematic drawing of the photoinduced intramolecular charge separation steps in **1-Oct** (i and ii), followed by the intermolecular electron transfer (iii) in mitochondria.

and long-lived photoinduction of CS.[18] Using the Fc-ZnP-C_{60} framework is also beneficial for suppressing the effects of $^3O_2$ during illumination because the triplet excited state lifetime is drastically shortened because of the transition to the energetically lower-lying charge separated state. Using **1-Me**, we were able to change cell membrane potentials and related neural activity by photocontrol.[17,20,21] This result encouraged us to explore additional applications of the Fc-ZnP-C_{60} analogue and the other donor-acceptor linked molecules that could be associated with highly efficient intramolecular and intermolecular ET reactions in biological system for use as photofunctional molecular tools.

In this study, we report on the design and synthesis of a donor-acceptor linked molecule (**1-Oct**) (Fig. 1) for use in the efficient photogeneration of a reduced acceptor (i.e. C_{60}) that can further participate in site-specific reductive reactions in mitochondria of living cells (Fig. 2). **1-Oct** was successfully delivered to the mitochondria of HeLa cells by a sophisticated drug delivery carrier that we refer to as MITO-Porter,[22] and demonstrated its capability to generate O_2^{-} in free from the generation of $^1O_2$ as the result of an ET reaction of the photoexcited **1-Oct**. Because the mitochondrion is an indispensable cellular organelle that is responsible for the production of the majority of the cell's energy supply and for the induction of cell death, such as apoptosis or necrosis, was set as the target, it provided us with an opportunity to evaluate its use to trigger a cellular response as the result of the photoinduced reductive reaction induced by **1-Oct**.

Experimental

Materials:

C_{60} (99.98%) was obtained from MTR Ltd. (OH, USA), and was used as-received. COATSOME EL-11-A (NOF co., Tokyo, Japan) (Lipid composition: POPC:Cholesterol:POPG = 30:40:30 mol%. unilamellar vesicle with high monodispersity) was obtained from NOF Co. (Japan). All other solvents and chemicals were of reagent-grade quality, were purchased commercially, and were used without further purification unless otherwise noted. Dulbecco's phosphate buffered saline (PBS) and Hank's Balanced Salt Solution (HBSS) were obtained from Thermo Fisher Scientific Inc. (MA, USA). Cell culture dishes and glass bottom dishes were purchased from Corning Inc. (MA, USA).

Synthesis:

Details are described in the Electronic Supplementary Information.

Incorporation of the Triads into COATSOME:

To an aqueous solution of COATSOME EL-11-A, a 1mM DMSO solution of **1-Me** or **1-Oct** was added at a concentration of 2.0 mol% as well as 1.0 v% relative to the lipids, and the solution and incubated at 37˚C. Incorporation was monitored by following the change in the absorbance of the Soret band. The incorporation was typically completed within 1 h.

Nanosecond TA Measurements:

Nanosecond time-resolved TA measurements were carried out using the laser system (Unisoku Co., Ltd., Osaka, Japan). Solvents were deaerated by argon bubbling for 5 min before measurements. A solution containing the triads or a mixture of the triads and COATSOME EL-11-A (molar ratio: 1/50) was excited by a Panther OPO pumped by a Nd:YAG laser (Continuum SLII-10, 4-6 ns fwhm), and the photodynamics were monitored by continuous exposure to a xenon lamp (150 W) as a probe light and a photomultiplier tube (Hamamatsu 2949) as a detector. The instrument response function (IRF) for this system is less than 10 ns (ca. 9 ns). The CS yields (Φ) in Table 1 were obtained by the comparative method,[17,23] which uses nanosecond TA spectra and the following equation:

$$\Phi = \Phi_{ref} \times \frac{\Delta OD_{max\text{-}sample}}{\Delta OD_{max\text{-}ref}}$$

where Φ_{ref} is the CS yield of the reference compound (0.99 for **Fc-ZnP-C$_{60}$-ref** in PhCN)[18], $\Phi OD_{max\text{-}sample}$ and $\Phi OD_{max\text{-}ref}$ are the maximum ΦOD intensities at 1000 nm of the compound of interest and the reference compound. Differences in molar extinction coefficients and the influence of the aggregation in the solvent systems are taken into account with the data for the fullerene radical anion obtained in the previous study.[17] Standard error of the data obtained here is less than 5%.

Detection of Photoinduced Superoxide in a Cuvette:

Photoinduced generation of superoxide was detected with MitoSOX (Thermo Fisher Scientific Inc., MA, USA) following the manufacture's protocol. Briefly, 0.12 μM of the compound (in cases of using the MITO-Porter, namely **1-Oct/MP** or **neg/MP**, 12 μM based on the lipids of **MP**, which contained 0.12 μM of **1-Oct**, was used) and 2.0 μM MitoSOX in deionized water was irradiated in a cuvette by Xe lamp (400 mJ cm^{-2}) with a band-pass filter (430-440 nm). The resulting solutions were immediately subjected to the spectrofluorometer with an excitation wavelength of 490 nm. The measurements were repeated for three times at least and results were statistically processed using Igor Pro v6.3 using a one-way ANOVA with a Dunnett's post *hoc* test for significance.

Detection of Photoinduced Singlet Oxygen:

Detection of Reactive oxygen species (ROS) with Singlet Oxygen Sensor Green (SOSG) reagent (Thermo Fisher Scientific Inc., MA, USA) was performed following manufacture's protocol. Briefly, a compound and 5.0 μM SOSG in deionized water were irradiated in a cuvette by a Xe lamp (400 mJ cm^{-2}) with a band-pass filter (430-440 nm). The resulting solutions were immediately subjected to the spectrofluorometer with an excitation wavelength of 490 nm. The measurements were repeated for three times at least and results were statistically processed using Igor Pro v6.3 using a one-way ANOVA with a Dunnett's post *hoc* test for significance.

Construction of the MITO-Porter with Other Compounds Incorporated:

1-Oct/MP, in which **1-Oct** is located in the lipid membranes of the MITO-Porter (**MP**), was prepared by the lipid film hydration method.[22,29] Lipid films were formed on the bottom of a glass tube by evaporating a 500 μL of $CHCl_3$/EtOH solution (1/1, v/v) containing 1.10 μmol of lipid [DOPE/SM = 9:2 (molar ratio)] and **1-Oct** (1.0 mol% of the total lipids). For experiments with microscopes, DiD (0.10 mol% of the total lipids) was also added here because of the intracellular concentration of **1-Oct** was so low that it was not possible to obtain an analyzable fluorescence signal in such concentration.

Next, 500 μL of 10 mM HEPES buffer with 290 mM glucose (pH 7.4) was added to the lipid film, followed by incubation at room temperature for 15 min to hydrate the lipids. The lipid film was then sonicated for 1 min in a bath-type sonicator (85 W, Aiwa Co., Tokyo, Japan) and the STR-R8 solution (10 mol% of the total lipids) was added to the suspension to produce **1-Oct/MP**. A MITO-Porter without **1-Oct** was also prepared for a reference (**neg/MP**) by the same procedure in the absence of **1-Oct**.

HeLa Cell Culture:

HeLa cells were cultured in Dulbecco's modified Eagle's minimal essential medium (DMEM) with low glucose (Sigma-Aldrich) supplemented with 10% Fetal bovine serum (FBS) (Japan Bioserum, Hiroshima, Japan) supplemented with 60 U/mL penicillin and 60 μg/mL streptomycin. The cells were cultured in 5% CO_2 and 95% air, and were passaged every 3–4 days. HeLa cells were used for the following experiments under these culturing conditions, unless stated otherwise.

Confocal Laser Microscopy Observations:

HeLa cells were cultured on a glass bottom dish. After 1 day, the medium was removed, cells were washed twice with HBSS(+) and the dish was then filled with serum free culture medium. **1-Oct/MP** or **neg/MP** was then added to the dish (final concentration of the total lipids of the MITO-Porter: 1.0–50 μM). The cells were then incubated in phenol red-free medium without serum under an atmosphere of 5% CO_2/air at 37◦C. After a 1 h incubation, the medium was replaced with fresh phenol red-free medium containing serum. After a further 100 min, the medium was replaced with fresh medium containing each of the fluorescent reagents, and the cells were incubated for additional 10 min to allow the mitochondria to be stained.

The cells were then washed with phenol red-free medium containing serum, and then observed by Zeiss LSM780 (Carl Zeiss Microscopy GmbH, Jena, Germany), which equips a 40× oil objective lens (NA 0.75), GaAsP (32 ch) array and CW lasers. The cells were illuminated by a 473 nm light from laser for detecting MitoTracker Green FM or MitoSOX, a 533 nm light for MitoTracker Orange CM-H2TMRos, and a 633 nm light for detecting DiD.

Confocal Laser Microscopy Observations without MITO-Porter:

After culturing of HeLa cells for 1 day on a glass bottom dish, the medium was removed, cells were washed twice with HBSS(+) and then the dish was filled with serum free culture

medium. A 1 mM solution of **1-Oct** (in DMSO/H_2O, 1/99, v/v) was added to the dish (final concentration of **1-Oct** in the dish: 10 μM). The cells were then incubated in phenol red-free medium without serum under an atmosphere of 5% CO_2/air at 37◦C. After a 1 h incubation, the medium was replaced with fresh phenol red-free medium containing serum. After a further 100 min, the medium was replaced with fresh medium containing each of the fluorescent reagents, and the cells were incubated for 10 min to allow the mitochondria to be stained. The cells were then washed with phenol red-free medium containing serum, and observed using the microscope. The cells were illuminated by a 430 nm light from diode laser for detecting **1-Oct**, a 473 nm light for MitoTracker Green FM, wheat germ agglutinin (WGA)-Alexa Fluor488 conjugate, or LysoTracker Green DND-26, and a 633 nm light for detecting DiD. Although fluorescence from **1-Oct** is weak, it could be detected by a GaAsP detector with a high sensitivity in the present case by using 10 μM of **1-Oct**.

Calculation of Weighted Co-localization Coefficients:

The Zeiss LSM780 Zen software was used to measure the weighted colocalization from three separate experiments. The weighted colocalization coefficients take into account the intensity value of the summed pixels. The weighted colocalization coefficients use the same equation as the colocalization coefficients,[25] but the value for each pixel is equal to its intensity value. Their values will range from 0 to 1, where 1 indicates the perfect colocalization. In this analysis, a pixel with a bright intensity represents a higher number of fluorophores than a pixel with a low intensity. To obtain the coefficients, several microscopic images were randomly selected and colocalization coefficients were first obtained from the cells in the images (n = 10) and finally statistically analyzed to obtain the coefficients with a standard deviation (1SD).

Detection of Photoinduced Apoptosis and Necrosis:

Cell apoptosis/necrosis was detected using an Annexin V-FITC Apoptosis Kit (BioVision, Inc., CA, USA), which contains an Annexin V-FITC conjugate for early apoptosis detection and propidium iodide (PI) for detecting late apoptosis and necrosis, according to the manufacture's protocol. Briefly, the cells were seeded on a black bottom 96 well plate with 5.0×10^3 cells mL^{-1} and cultured for 1 day. The medium was then removed, the dish was washed with HBSS(+) twice and filled with serum free culture medium. Then, the MITO-Porter samples were added to the HeLa cells (final concentration based on the total lipids of MITO-Porter, 5.0 μM). The cells were then incubated in phenol red-free medium without serum under an atmosphere of 5% CO_2/air at 37°C. After 1 h incubation, the medium was replaced with fresh phenol red-free medium containing serum. After a further 100 min, the medium was replaced with fresh medium containing each of the fluorescent reagents, and the cells were incubated for 10 min to allow the mitochondria to be stained. The cells were then washed once and filled with phenol red-free medium containing serum, and then used for the assay as below.

The cells were illuminated by a Xe lamp (0.66 mW cm^{-2}, 430-440 nm) for 10 min (total 400 mJ cm^{-2}). After the medium was replaced to HBSS(+), the cells were treated with the Annexin V-FITC/PI solution, incubated for 10 min at room temperature, and then observed by a Gemini XPS Microplate Reader (MOLECULAR DEVEICE Inc.) with double excitation at 475 nm for Annexin V-FITC and 538 nm for PI with band-filters of 485-515 nm and 544-570 nm. The ratios of dead cells were calibrated with confocal laser microscopy experiments using Fluoview-10i (Olympus) in negative control conditions and in positive control conditions, respectively. Negative control experiments were performed with the cells prepared as described above, but in the absence of the MITO-Porter samples. Positive control experiments were performed by culturing the cells in 20% DMSO for the necrosis detection. For the detection of early apoptosis, the ratio was calibrated by the results of 50 μM **1-Oct/MP**. Fluorescent cells were counted as cells in early apoptosis (green) or those in late apoptosis or necrosis (red or yellow). For one experiment, more than 500 cells were counted from three randomly chosen images (more than 150 cells per an image). Assays were performed in triplicate and the results were analyzed statistically using Igor Pro v6.3 using a one-way ANOVA with a Dunnett's post *hoc* test for significance.

Results and discussion

Design, synthesis, and electronic properties of the molecule:

Very recently, our group created a series of electron donor-acceptor linked amphiphilic molecules based on the Fc-ZnP-C_{60} analogue.[17,21] In one of the molecules (**1-Me**) (Fig. 1), photoinduced CS takes place to form the long-lived charge-separated state (Fc^+-ZnP-$C_{60}^{\bullet-}$) with moderate quantum yields in highly polar solvents (Φ = 0.57 in DMSO/H_2O, 1/99, v/v) and in an artificial lipid bilayer system (Φ = 0.27 in COATSOME whose composition is POPC:Cholesterol:POPG = 30:40:30 mol%). One can envision that the electrochemically high-reducing capability of $C_{60}^{\bullet-}$ (*vide infra*) and a long lifetime (10^{-5}–10^{-4} s^{-1}) of the charge-separated state of **1-Me** would lead to intermolecular ET reactions in biological environments.

To improve the CS quantum yield in the cell membrane, we prepared a new type of Fc-ZnP-C_{60} molecule in which an octyl chain was introduced into the pyrolidine ring on the C_{60} moiety (**1-Oct**) (Figs. 1 and S2 ESI†). Because intermolecular π-π interactions of C_{60} moiety are mainly responsible for the development of aggregation resulting in a decreased CS quantum yield of **1-Me**,[17] replacing the methyl group on the pyrrolidine ring with a long alkyl chain like octyl moiety was anticipated to suppress this undesirable aggregation and would decrease the CS yield by the intermolecular cancelling of CS.[16,24] Although this type of elongation of the side chain (i.e. extension with a heptyl moiety) is known to have little influence on the electronic properties of molecules in organic solvents where the molecules exist in monomeric form, it is also known that such long alkyl chain can have remarkable effect in highly polar solvents, in micelles, or in the solid state,

in which fullerene derivatives would undergo extensive aggregation.[26]

A comparison of the absorption spectra revealed that the intensity of the Soret-band for **1-Oct** is larger than that for **1-Me** in DMSO/H_2O (1/99, v/v) and in the COATSOME, respectively (Fig. S3). This result indicates that **1-Me** would likely have a higher tendency to form aggregates than **1-Oct** in which the octyl chain would effectively suppress the aggregation.[27]

Photoinduced intramolecular and intermolecular electron transfer properties:

Electrochemical measurements revealed that the first reduction potentials of the C_{60} moiety (**1-Me**: –0.25 V, **1-Oct**: –0.40 V, vs. SHE) (Fig. S4 and Table S1) are feasible to reduce molecular oxygen (E_{red} = −0.15 V) in their photoinduced charge separated states (Schemes S1 and S2). **1-Oct** demonstrated a remarkably lower reduction potential (–0.40 V) compared to **1-Me** (–0.25 V) in aqueous solution. Since the aggregation of C_{60} is known to cause an anodic shift in the reduction potential,[28] this result indicates that the octyl chain of **1-Oct** is effective in partially suppressing the aggregation caused by the presence of the C_{60} moieties, leading to a cathodic shift in the reduction potential of **1-Oct**. The lower reduction potential of **1-Oct** compared to that of **1-Me** is energetically more favorable for causing the photoinduced reduction of O_2 from the charge-separated state (i.e. Fc^+-Por-$C_{60}^{\bullet-}$) (Scheme S2). In contrast, the moderate oxidizing potential of the Fc moiety (**1-Me**: +0.36 V, **1-Oct**: +0.40 V) would be advantageous for avoiding undesired oxidation of unsaturated lipid molecules (mono-unsaturated lipid: E_{ox} ~ +0.6 V)[29] and the other endogenous biomolecules[28] by the oxidized Fc moiety (Fc^+) as a side reaction. These results suggested that **1-Oct** would be a more suitable molecule than **1-Me** for participating in an efficient photoinduced reductive reaction in a cellular environment.

Nanosecond transient absorption measurements were carried out to observe the formation of Fc^+-ZnP-$C_{60}^{\bullet-}$ by illumination. Photoinduced CS yields were also determined by monitoring the signal at 1000 nm (Table 1, Figs. S5 and S6),[17,23] which is a finger print of $C_{60}^{\bullet-}$ because of the photoinduced CS, namely the initial ET from ^{1}ZnP* to C_{60} followed by a second ET from Fc to $ZnP^{\bullet+}$ to generate Fc^+-ZnP-$C_{60}^{\bullet-}$. Note that the Fc^+ was not detected due to its low molar extinction coefficient at 800 nm.[18] Reflecting the suppression of aggregation, higher CS yields of **1-Oct** were obtained, compared to those of **1-Me** both in DMSO/H_2O and COATSOME, which mimics the cellular environment.

Feasible electron transfer from $C_{60}^{\bullet-}$ to O_2 was implied by the fact that the CS yields and lifetimes in aerated DMSO/H_2O were remarkably smaller and shorter than those in the deaerated solution (Fig. S6). Therefore, the abilities of the molecules to generate O_2^- were investigated in an aqueous solution by using MitoSOX, a commercially available fluorogenic reagent for the selective sensing of O_2^- (Fig. 3). After illumination (430-440 nm, 400 mJ cm^{-2}), **1-Oct** showed larger generation capability of O_2^- than that of **1-Me**.

Table 1 Charge recombination rate constant (k_{CR}) and CS yield (Φ)[a]

medium	compound	k_{CR1} /10^5 s^{-1} (/%)[b]	k_{CR2} /10^4 s^{-1} (/%)[b]	Φ_{CS}[c]
DMSO/H_2O[d]	**1-Me**	4.5 (58)	1.4 (42)	0.57
	1-Oct	10.5 (73)	1.5 (27)	0.67
COATSOME in H_2O	**1-Me**	2.5 (58)	1.1 (42)	0.27
	1-Oct	3.6 (50)	1.5 (50)	0.35

[a]Data were obtained from the decay profiles of $C_{60}^{\bullet-}$ (λ_{ex}= 450 nm, λ_{obs}=1000 nm) by bi-exponential fitting. Standard errors for the data shown here are less than 5%. [b]Values in parentheses denote amplitude ratios. [c]Values were obtained by the comparative method with taking account of the different molar absorption coefficients derived from the solvents that were used for the TA measurements.[17,23] [d]1/99, v/v.

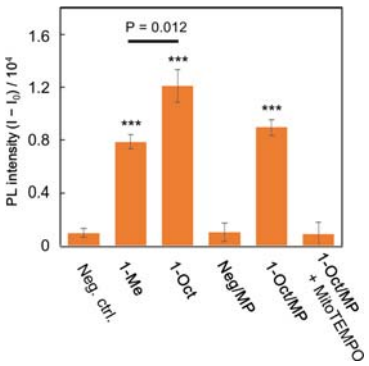

Fig. 3 Generation ability of O_2^-, as determined by the change in photoluminescence (PL) intensity of MitoSOX after illumination (*hv*: 430-440 nm, 400 mJ cm^{-2}) in H_2O. Error bars indicate the standard deviation (1SD) (n = 4). Statistically significant differences between the negative control and each condition are illustrated with asterisks (*P < 0.05, **P < 0.01, ***P < 0.001).

Meanwhile, an assay using Singlet Oxygen Sensor Green (SOSG), which selectively detects $^1O_2$, verified that neither **1-Oct** nor **1-Me** generate significant amounts of $^1O_2$ (Fig. S7). We therefore concluded that **1-Oct** is the most suitable photosensitizing molecule for the exclusive generation of O_2^-.

Mitochondrial delivery of the molecule with a nano-carrier:

The mitochondrion was selected as a target for the site-specific donation of electrons from photoexcited **1-Oct** in cells, because it is an important organelle that governs the fate of cells.[10,11] HeLa cells were used in the present study because it is a well-studied cell system and the cell is a model for developing cancer therapeutics. Owing to the relatively high hydrophobic as well as lipophilic nature of **1-Oct**, **1-Oct** itself is not intrinsically able to penetrate the cell membrane and is therefore not capable of reaching mitochondria. Confocal laser microscopic observations revealed that **1-Oct** itself accumulates on the cell membrane, and can be transported to lysosomes probably by endocytosis (Figs. 4a and S8). To deliver **1-Oct** to mitochondria, the MITO-Porter was used as a

carrier.[22] The MITO-Porter is a liposome-based mitochondrial delivery system that functions by penetrating the outer cell membrane, followed by fusion with the mitochondrial membrane. We recently reported that the MITO-Porter possesses sufficient targeting and transporting capabilities with respect to mitochondria and can carries small molecules and biological molecules including DNA, and RNA. [22,31-33] In addition, the MITO-Porter has been reported to be an effective carrier for *in vivo* applications.[34] These features encouraged us to use it as a potential promising carrier for the delivery of photofunctional molecules such as **1-Oct**.

1-Oct was incorporated into the MITO-Porter (**MP**). The resulting conjugate is referred to as **1-Oct/MP** (**1-Oct** was contained 1.0 mol% relative to the total lipids of **MP**). For experiments of using a confocal laser microscope, a fluorescent dye DiD (0.10 mol% of the total lipids) was also incorporated for use in tracking because of the small intracellular concentration (<0.5 μM) of **1-Oct** which did not produce analyzable fluorescence signals under the present conditions. On the other hand, when **1-Oct** itself, in the absence of the MITO-Porter, was applied to the cells in high concentrations, as shown above (10 μM for a dish) (Figs. 4a and S8), the fluorescence from **1-Oct** could be detected by the GaAsP detector with a high degree of sensitivity. Steady state fluorescence spectra confirmed that the intramolecular energy transfer from **1-Oct** to DiD does not occur in the MITO-Porter (Fig. S9). An empty carrier (**neg/MP**) was also prepared as a reference.

Confocal microscopy images clearly confirmed that **1-Oct/MP** selectively delivered **1-Oct** to mitochondria (Figs. 4b and 4c). Weighted co-localization coefficients (a coefficient equal to 1.00 indicates perfect co-localization. See the Experimental Section for details) obtained based on observation with MitoTracker Green FM were found to be 0.76 ± 0.12 for **1-Oct/MP**, 0.77 ± 0.06 for **neg/MP**, and 0.00 ± 0.00 for **1-Oct** in the absence of the MITO-Porter. The delivery efficiencies were comparable or even higher than those for our previously reported MITO-Porter systems.[35] Because the MITO-Porter contained the lipids that are highly fusogenic toward the mitochondrial membrane,[21] **1-Oct** would be expected to be transported to the mitochondria by MITO-Porter and, when the MITO-Porter fuses with the mitochondrial membrane, **1-Oct** would also be transferred to the membrane. Therefore, the photoinduced effects from **1-Oct** would be expected to occur in and/or on the mitochondrial membrane.

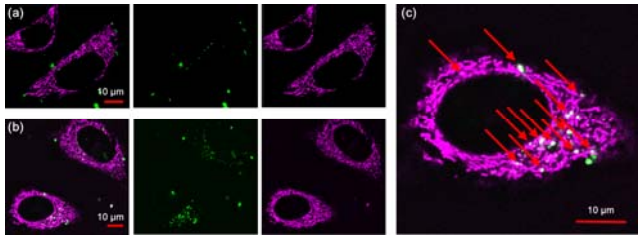

Fig. 4 Confocal microscopy images of HeLa cells that were stained with MitoTracker Green FM and treated with (a) **1-Oct**, in the absence of the MITO-Porter, and (b) **1-Oct/MP**, which contained DiD. Merged image (left), compounds (green, center), and MitoTracker Green FM (magenta, right). (c) Magnification of the merged image of (b). Red arrows indicate strong overlapping points (white) of the compounds and the fluorescent reagent.

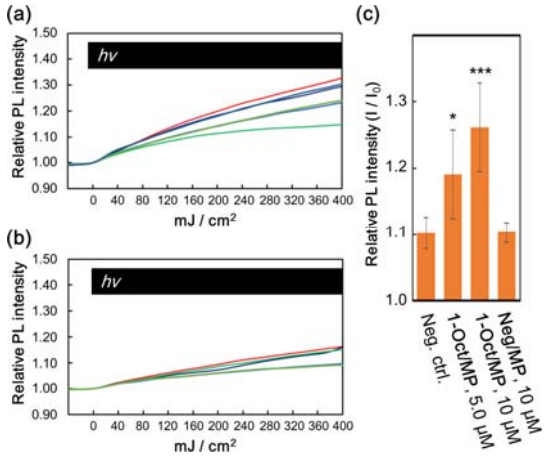

Fig. 5 Traces showing the change in photoluminescence (PL) of the MitoSOX, which detects (O_2^-), in the mitochondria of HeLa cells upon illumination (*hv*: 430-440 nm) caused by (a) **1-Oct/MP** and (b) **neg/MP**. Both compounds were individually used at a concentration of 10 μM based on the lipids of **MP**. (c) Generation of O_2^- determined by the change in the PL intensity of MitoSOX after the illumination (*hv*: 430-440 nm, 400 mJ cm^{-2}) of HeLa cells. The indicated concentrations are based on the lipids of the Mito-Porter. Error bars indicate standard deviation (1SD) (n = 6). Statistically significant differences between the negative control and each condition are illustrated with asterisks (*P < 0.05, ***P < 0.001).

Photoinduced electron transfer in mitochondria from the molecule:

It was first confirmed in aqueous solution that **1-Oct/MP** is capable of generating remarkably large amounts of O_2^- when illuminated (Fig. 3), and the resulting O_2^- was effectively quenched by MitoTEMPO, a commercially available O_2^- quencher. The intracellular electron-donating capability of **1-Oct/MP** in mitochondria was then examined. After incorporating **1-Oct/MP** into the mitochondria, a significant

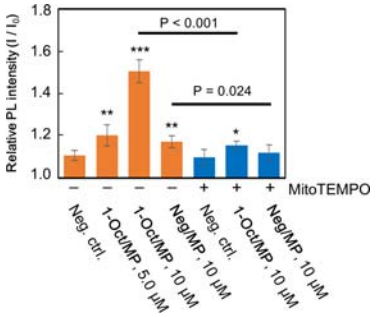

Fig. 6 Comparison of the abilities to generate ROS in the presence and absence of the MitoTEMPO, a mitochondria specific O_2^- quencher. Generation of ROS was detected by the change in photoluminescence (PL) intensity of MitoTracker Orange CM-H2TMRos after illumination (*hv*: 430-440 nm, 400 mJ cm^{-2}) of HeLa cells. The indicated concentrations are based on the lipids of the Mito-Porter. Error bars indicate standard deviation (1SD) (n = 6). Statistically significant differences between the negative control and each condition are illustrated with asterisks (*P < 0.05, **P < 0.01, ***P < 0.001).

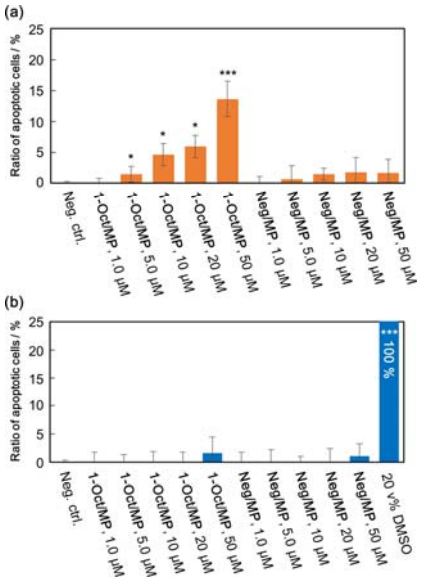

Fig. 7 Ability to induce apoptosis of HeLa cells (a) with and (b) without illumination (*hv*: 430-440 nm, 400 mJ cm^{-2}). The indicated concentrations are based on the lipids of the MITO-Porter. Error bars indicate S.D. (n = 4). Statistically significant differences between the negative control and each condition are illustrated with asterisks (*P < 0.05, ***P < 0.001). The positive control condition is incubation of HeLa cells in culture medium containing 20 v% of DMSO for 2 h at 37°C prior to the assays.

generation of O_2^- was detected by MitoSOX, a fluorogenic reagent that exclusively detects O_2^- in mitochondria, with illumination (Figs. 5 and S10). In sharp contrast, negligible amounts of O_2^- were generated by **neg/MP**, indicating that the effective photoinduced reductive reaction caused by **1-Oct/MP** occurred inside the mitochondria. The influence of **1-Oct/MP** outside mitochondria was also assessed by using MitoTracker Orange CM-H2TMRos, an organelle non-specific fluorogenic reagent that is nonfluorescent in its reduced form but acquires fluorescent properties after oxidization by various kinds of ROS, followed by selective accumulation in mitochondria (Figs. 6 and S11). In the cells treated with **neg/MP** and negative control conditions, a detectable increase in fluorescence on illumination was observed, which can be attributed to the production of ROS by intrinsic biomolecules in the cells, such as flavin derivatives, protoporphyrins and their precursors.[36,37] In the case of cells that had been treated with **1-Oct/MP**, a significant large increase of fluorescence as a result of light irradiation was detected, indicating that ROS were generated somewhere in the cells. Because the ROS generation by **1-Oct/MP** was effectively quenched by the addition of MitoTEMPO, this suggests that the ROS generation caused by **1-Oct/MP** occurs specifically in mitochondria and the dominant ROS is O_2^-. Although a small amount of ROS was generated by **1-Oct/MP** in the presence of MitoTEMPO, this could be attributed to the plausible escape of **1-Oct** during the apoptosis process (*vide infra*). We therefore concluded that selective reduction was induced by the illumination of **1-Oct/MP** in the mitochondria resulting the generation of O_2^-.

Finally, apoptotic cell death was induced by photoirradiation in order to evaluate the utility of the photoinduced reductive reaction in mitochondria by **1-Oct/MP** because apoptotic cell death is an unambiguous mitochondrial cell signalling response as a result of intracellular signalling by O_2^-.[11] An Annexin-V/propidium iodide kit was used to detect early apoptosis, late apoptosis and necrosis. After illumination, a high concentration of **1-Oct/MP** (≥ 5 μM base on the lipids of **MP**) induced a significant level of apoptosis (Fig. 7). In sharp contrast, no significant induction ability was observed in the case of **neg/MP** (conc. ≥ 10 μM). Meanwhile, both **1-Oct/MP** and **neg/MP** did not cause remarkable necrotic cell death (Fig. S12). Supported by the fact that the exclusive generation of O_2^- in mitochondria occurred *via* **1-Oct/MP**, as mentioned above, this apoptotic death arose from the site-specific reduction of O_2 causing O_2^- generation by the illumination of **1-Oct** in the mitochondria.

Conclusions

The use of a combination of **1-Oct** and MITO-Porter resulted in the successful incorporation of a donor-acceptor linked molecule, which possesses excellent intrinsic photoinduced CS properties, into mitochondria. The delivery of **1-Oct** specifically to mitochondria permitted a photoinduced intermolecular ET reaction with O_2 to occur in mitochondria, which was derived from the efficient photoinduced CS associated with **1-Oct**. The targeted generation of O_2^- in the mitochondria enabled us to induce apoptosis of HeLa cells. These results pave the way for developing non-invasive photocontrol methods based on redox reactions at specific locations with timely control methods for oxido-reductive cell signaling. Since the MITO-Porter can serve as a promising carrier for *in vivo* usage,[34] the present work provides new opportunities for establishing novel methodology for controlling cellular functions by light for developing phototherapeutic molecular tools.

Conflict of interest

There are no conflicts to declare.

Acknowledgements

This work was supported by Grants-in-Aid for Scientific Research (S) (25220801 to H.I and Y.T.), (B) (26282131 to Y.Y), (C) (15K05563 to Y.T.), and Grant-in-Aid for Challenging Exploratory Research (25560219 to Y.Y.) from MEXT, Japan. The iCeMS is supported by the World Premier International Research Center Initiative. Y.T. wishes to acknowledge E. Hirata for fruitful discussions regarding experimental design. We are grateful to the CeMI for microscopic measurements and to Y. Fukuda, K. Nakamura and E. Kawamura for their dedicated cooperation in preparing the MITO-Porter used in the study.

Notes and references

1 C. Brieke, F. Rohrbach, A. Gottschalk, G. Mayer and A. Heckel, *Angew. Chem. Int. Ed.*, 2012, **51**, 8446-8476.
2 A. M. Packer, B. Roska and M. Hausser, *Nat. Neurosci.*, 2013, **16**, 805-815.
3 W. J. Wedemeyer, E. Welker, M. Narayan and H. A. Scheraga, *Biochemistry*, 2000, **39**, 4207-4216.
4 C. X. C. Santos, L. Y. Tanaka, J. Wosniak and F. R. M. Laurindo, *Antioxid. Redox Signal*, 2009, **11**, 2409-2427.
5 Y. Takagi, T. Tokime, K. Nozaki, Y. Gon, H. Kikuchi and J. Yodoi, *J. Cereb. Blood Flow Metab.*, 1998, **18**, 206-214.
6 A. U. Igamberdiev, N. V. Bykova, P. J. Lea and P. Gardestrom, *Physiol. Plant.*, 2001, **111**, 427-438.
7 A. Willie, P. S. Stayton, S. G. Sligar, B. Durham and F. Millett, *Biochemistry*, 1992, **31**, 7237-7242.
8 N. F. Polizzi, M. J. Eibling, J. M. Perez-Aguilar, J. Rawson, C. J. Lanci, H. C. Fry, D. N. Beratan, J. G. Saven and M. J. Therien, *J. Am. Chem. Soc.*, 2016, **138**, 2130-2133.
9 A. M. Lifschitz, R. M. Young, J. Mendez-Arroyo, C. L. Stern, C. M. McGuirk, M. R. Wasielewski and C. A. Mirkin, *Nat. Commun.*, 2015, **6**, 6541.
10 D. R. Green and J. C. Reed, *Science*, 1998, **281**, 1309-1312.
11 M. Madesh and G. Hajnoczky, *J. Cell Biol.*, 2001, **155**, 1003-1015.
12 Y. A. Suh, R. S. Arnold, B. Lassegue, J. Shi, X. X. Xu, D. Sorescu, A. B. Chung, K. K. Griendling and J. D. Lambeth, *Nature*, 1999, **401**, 79-82.
13 M. Liu, H. Liu and S. C. Dudley, *Circul. Res.*, 2010, **107**, 967-974.
14 M. E. Bulina, K. A. Lukyanov, O. V. Britanova, D. Onichtchouk, S. Lukyanov and D. M. Chudakov, *Nat. Protoc.*, 2006, **1**, 947-953.
15 W. H. Lei, J. F. Xie, Y. J. Hou, G. Y. Jiang, H. Y. Zhang, P. F. Wang, X. S. Wang and B. W. Zhang, *J. Photoch. Photobio. B*, 2010, **98**, 167-171.
16 C. Schweitzer and R. Schmidt, *Chem. Rev.*, 2003, **103**, 1685-1757.
17 Y. Takano, T. Numata, K. Fujishima, K. Miyake, K. Nakao, W. D. Grove, R. Inoue, M. Kengaku, S. Sakaki, Y. Mori, T. Murakami and H. Imahori, *Chem. Sci.*, 2016, **7**, 3331-3337.
18 H. Imahori, K. Tamaki, D. M. Guldi, C. P. Luo, M. Fujitsuka, O. Ito, Y. Sakata and S. Fukuzumi, *J. Am. Chem. Soc.*, 2001, **123**, 2607-2617.
19 H. Imahori, H. Yamada, Y. Nishimura, I. Yamazaki and Y. Sakata, *J. Phys. Chem. B*, 2000, **104**, 2099-2108.
20 T. Numata, T. Murakami, F. Kawashima, N. Morone, J. E. Heuser, Y. Takano, K. Ohkubo, S. Fukuzumi, Y. Mori and H. Imahori, *J. Am. Chem. Soc.*, 2012, **134**, 6092-6095.
21 N. Cai, Y. Takano, T. Numata, R. Inoue, Y. Mori, T. Murakami and H. Imahori, *J. Phys. Chem. C*, 2017, **121**, 17457-17465.
22 Y. Yamada, H. Akita, H. Kamiya, K. Kogure, T. Yamamoto, Y. Shinohara, K. Yamashita, H. Kobayashi, H. Kikuchi and H. Harashima, *BBA-Biomembranes*, 2008, **1778**, 423-432.
23 T. Higashino, T. Yamada, M. Yamamoto, A. Furube, N. V. Tkachenko, T. Miura, Y. Kobori, R. Jono, K. Yamashita and H. Imahori, *Angew. Chem. Int. Ed.*, 2016, **55**, 629-633.
24 E. M. M. Manders, F. J. Verbeek and J. A. Aten, *J. Microsc.*, 1993, **169**, 375-382.
25 S. Fukuzumi, R. Hanazaki, H. Kotani and K. Ohkubo, *J. Am. Chem. Soc.*, 2010, **132**, 11002-11003.
26 L. P. Zheng, Q. M. Zhou, X. Y. Deng, M. Yuan, G. Yu and Y. Cao, *J. Phys. Chem. B*, 2004, **108**, 11921-11926.
27 K. Komagoe, K. Tamagake and T. Katsu, *Chem. Pharm. Bull.*, 2006, **54**, 1004-1009.
28 S. R. Chae, A. R. Badireddy, J. F. Budarz, S. H. Lin, Y. Xiao, M. Therezien and M. R. Wiesner, *ACS Nano*, 2010, **4**, 5011-5018.
29 Y. Y. Tyurina, V. Kini, V. A. Tyurin, I. I. Vlasova, J. F. Jiang, A. A. Kapralov, N. A. Belikova, J. C. Yalowich, I. V. Kurnikov and V. E. Kagan, *Mol. Pharmacol.*, 2006, **70**, 706-717.
30 M. Born, P. A. Carrupt, R. Zini, F. Bree, J. P. Tillement, K. Hostettmann and B. Testa, *Helv. Chim. Acta*, 1996, **79**, 1147-1158.
31 Y. Yamada, K. Nakamura, R. Furukawa, E. Kawamura, T. Moriwaki, K. Matsumoto, K. Okuda, M. Shindo and H. Harashima, *J. Pharm. Sci.*, 2013, **102**, 1008-1015.
32 Y. Yasuzaki, Y. Yamada, T. Ishikawa and H. Harashima, *Mol. Pharm.*, 2015, **12**, 4311-4320.
33 Y. Yamada, R. Furukawa and H. Harashima, *J. Pharm. Sci.*, 2016, **105**, 1705-1713.
34 Y. Yamada, K. Nakamura, J. Abe, M. Hyodo, S. Haga, M. Ozaki and H. Harashima, *J. Controlled Release*, 2015, **213**, 86-95.
35 Y. Yamada, H. Akita and H. Harashima, *Method Enzymol.*, 2012, **509**, 301-326.
36 S. Chaudhuri, S. Batabyal, N. Polley and S. K. Pal, *J. Phys. Chem. A*, 2014, **118**, 3934-3943.
37 J. C. Kennedy and R. H. Pottier, *J. Photoch. Photobio. B*, 1992, **14**, 275-292.